forests

MDPI

Article

Aboveground Biomass Mapping and Fire Potential Severity Assessment: A Case Study for Eucalypts and Shrubland Areas in the Central Inland Region of Portugal

Cristina Alegria [1,2]

[1] Instituto Politécnico de Castelo Branco, Polytechnic University of Castelo Branco, 6000-084 Castelo Branco, Portugal; crisalegria@ipcb.pt
[2] CERNAS-IPCB—Pólo de Castelo Branco do Centro de Estudos de Recursos Naturais, Ambiente e Sociedade, Unidade de Investigação e Desenvolvimento do Instituto Politécnico de Castelo Branco, 6000-084 Castelo Branco, Portugal

Abstract: Shrubland and forestland covers are highly prone to fire. The Normalized Difference Vegetation Index (NDVI) has been widely used for biomass quantitative assessment. The objectives of this study were as follows: (1) to compute the NDVI annual curve for two types of land cover eucalypts and shrubland areas; (2) to collect field data in these two types of land cover to estimate aboveground biomass (AGB); and (3) to produce AGB maps for eucalypts and shrubland areas by modelling AGB with NDVI, validate them with other data sources, and to compare fuel loads with fire severity levels. A study area in the central inland region of Portugal was considered. The wildfire on 4 August 2023 was considered for burn severity levels assessment using the Normalized Burn Index (NRB). The Sentinel-2 MSI imagery was used to compute the NDVI for the years of 2022 and 2023 and the NBR for the pre-fire and post-fire dates. The NDVI annual curve for 2022 showed a minimum observed between July and August, in accordance with the climatological data, and allowed differentiating eucalypts from shrubland areas. Spectral signatures also confirmed this differentiation. The fitted linear models for AGB prediction using the NDVI imagery showed good fitting performances (R^2 of 0.76 and 0.77). The AGB maps provided a relevant decision support tool for forest management and for fire hazard and fire severity mitigation. Further research is needed using more robust datasets for an independent validation of the model.

Keywords: biomass components; carbon sequestration; NDVI-CV method; spectral signatures; fire hazard; burn severity levels

Citation: Alegria, C. Aboveground Biomass Mapping and Fire Potential Severity Assessment: A Case Study for Eucalypts and Shrubland Areas in the Central Inland Region of Portugal. *Forests* **2023**, *14*, 1795. https://doi.org/10.3390/f14091795

Academic Editor: Yihang Zhang

Received: 2 August 2023
Revised: 30 August 2023
Accepted: 1 September 2023
Published: 3 September 2023

1. Introduction

In most developed countries, land use area assessment is based on field measurement, and biomass stock is estimated from the national forest inventory [1]. Despite field data collection being the most accurate technique, it is costly, time-consuming, and impractical at a large scale when destructive data collection is needed for biomass quantification [2,3]. Therefore, forest biomass is commonly estimated by allometric functions through biomass components (e.g., stem, bark, branches, leaves, seeds, and roots) and describes the total dry weight of live trees per unit area by relating them to structural metrics such as stand composition and density, tree diameter at breast height, and tree total height [4,5].

Forest aboveground biomass estimation (AGB—e.g., stem, bark, branches, leaves, and seeds) serves as a basic component in studies to estimate forest ecosystems' carbon stocks and their changes, which mainly include trees as the most important element of and the largest living biomass reserves in forests [2–4,6]. Thus, forest AGB maps are important tools to monitor global carbon cycle and for climate studies. But they are also important to identify areas of high conservation priority—or with high intraspecific competition—with

a potential need for management treatments [4,6,7] and to estimate forest residues for biomass energy production [8].

During the past several decades, remote sensing has been widely used for biomass estimation due to its wide-area coverage capability in response to the limitations of field data collection on large scales. Nevertheless, field data remain indispensable to both remotely sensed data calibration and biomass estimation validation. To improve forest AGB estimation accuracy, the integration of field data with various remotely sensed data sources are being essayed (including optical, SAR—synthetic aperture radar, and LiDAR—light detection and ranging) [6,7].

Forest AGB can be mapped over an area of interest by linking plot-level forest inventories with remote sensing measurements related to forest canopy cover, structure, and composition [5]. Indeed, a strong statistical relationship is observed between several spectral vegetation indices (VIs) obtained by remotely sensing data and the AGB obtained from ground plots [2,3]. For instance, the Normalized Difference Vegetation Index (NDVI) has been widely used for a quantitative assessment of vegetation and biomass [7,9,10]. Indeed, the NDVI not only measures vegetation greenness in relation to the structural properties of plants (e.g., leaf area index and green biomass), but also to properties of vegetation productivity (e.g., absorbed photosynthetic active radiation and foliar nitrogen) [11]. For instance, the NDVI has been used with forest inventory data to model wood production and biomass [2,12–14].

The Portuguese territory is very rich in raw materials that can be used as sources of biomass. More than 60% of the mainland territory is occupied by forests (around 3.2 Mha) and by shrubland and pastures (around 2.8 Mha) [8,15]. According to the last National Forest Inventory (NFI 2015) statistics by the Instituto da Conservação da Natureza e das Florestas (ICNF), eucalypts are the most abundant species (*Eucalyptus* sp.; 26%; 845,000 ha), followed by cork oak (*Quercus suber* L.; 22%; 719,900 ha), maritime pine (*Pinus pinaster* Aiton; 22%; 713,300 ha), and holm oak (*Quercus rotundifolia* Lam.; 11%; 349,400 ha) [15].

In Portugal, eucalyptus are an exotic, light-demanding, and fast-growing species, mostly planted and managed through a coppice system of three short harvesting cycles (e.g., 10–12-year rotations) for high wood production and removal [16]. In eucalypts in industrial plantations, a high concentration of the main nutrients in each biomass component is observed, thus raising concerns about the removal of P, K, Ca, and Mg from sites during logging and in post-logging burns [17,18]. In order to minimize the impact of soil nutrients removal, it is highly recommended to retain both foliage and bark at the felling site [19,20].

According to the NFI 2015 statistics, eucalypts areas represent a biomass of 34.71 Gg in live trees (aboveground and roots), and shrubland and pasture areas represent a live biomass of 17.36 Gg, corresponding to a carbon sequestration of 63.64 Gg and 24.74 Gg CO_{2e}, respectively. Eucalyptus plantations (e.g., pure stands) represent an AGB of 21.70 Gg (39.78 Gg CO_{2e}) with an average of 31.51 Mg ha^{-1} (57.76 Mg ha^{-1} CO_{2e}) [15].

Shrubland and forestland covers are highly prone to fire. Portuguese forest stands are differentially prone to fire, with mature forests of broadleaved deciduous and mixed forests having a lower fire hazard compared to pure pine forests, eucalyptus plantations, or mixed pine and eucalyptus stands [21–23]. Four groups of fire hazards were identified by the authors of [21] for Portuguese forests based on an increasing order of fire potential risk: (1) open and tall forest types, and closed and tall *Quercus suber* and diverse forests; (2) closed, low woodlands of deciduous oaks, *Q. suber* and diverse forests, closed and tall *Pinus pinaster* woodland and tall *Eucalyptus globulus* plantations; (3) open and low forest types; and (4) dense, low stands of *P. pinaster*, *E. globulus*, and Acacia. Thus, the fire severity generally decreases as the species flammability decreases, the stand height increases (less fuel vertical continuity) and the stand density decreases (less fuel load) [21,24].

Currently, the official national fire hazard map by the Autoridade Florestal Nacional (AFN, currently renamed to ICNF) is based on a multiplicative model of the annual fire probability (annual burned areas maps) and fire susceptibility (slope, and land cover) [25]. Although fire susceptibility defines the fire potential severity, this model does not con-

sider fuel loads. In general, tall, open stands have a lower fire severity than short, close stands [21,23]. Indeed, fire severity describes the immediate effects of fire produced by the aboveground and belowground heat release pulses, and its assessment is based on biomass consumption and a visual evidence of heating and heat-inflicted injury to vegetation. However, spatial patterns in fire severity are determined by a complex interplay between forest composition and structure, weather, and topography, even under extreme meteorological conditions [23]. A high correlation has been observed between burn severity levels within burned areas using spectral indices computed from the Sentinel-2 imagery (e.g., the differenced Normalized Burn Ratio—dNBR) and the field measurements in burn areas. In fact, this is the methodological approach used by the European Forest Fire Information Service (EFFIS), under the Copernicus program, the main source of European wildfires information [26,27].

Thus, this research hypothesis was that the NDVI is a reliable predictor for mapping eucalypts and shrubland areas' AGB to provide a decision support tool for forest management and for fire hazard and fire severity mitigation. The objectives of this study were as follows: (1) to compute the NDVI annual curve for two types of land cover (eucalypts and shrubland areas); (2) to collect field data in these two types of land cover to estimate AGB; and (3) to produce AGB maps for eucalypts and shrubland areas by modelling AGB with NDVI, validate them with other data sources, and to compare fuel loads with fire severity levels using the NRB. A study area in the central inland Portugal region was considered. The Sentinel-2 MSI imagery was used to compute the NDVI for the years of 2022 and 2023 and the NBR for the pre-fire and post-fire dates. Field data allowed us to estimate AGB and to model this variable with NDVI. AGB maps were produced and validated. The wildfire on 4 August 2023 was used to compare fuel loads with fire severity levels.

2. Materials and Methods

2.1. Study Area

The study area is in the central inland Portugal region and is included in the intermunicipal community of Beira Baixa (CIMBB; 493,056 ha) that integrates six municipalities, namely: Oleiros (47,109 ha), Proença-a-Nova (39,540 ha), Vila Velha de Rodão (32,991 ha), Castelo Branco (143,819 ha), Idanha-a-Nova (141,633 ha), and Penamacor (56,370 ha) [28] (Figure 1a).

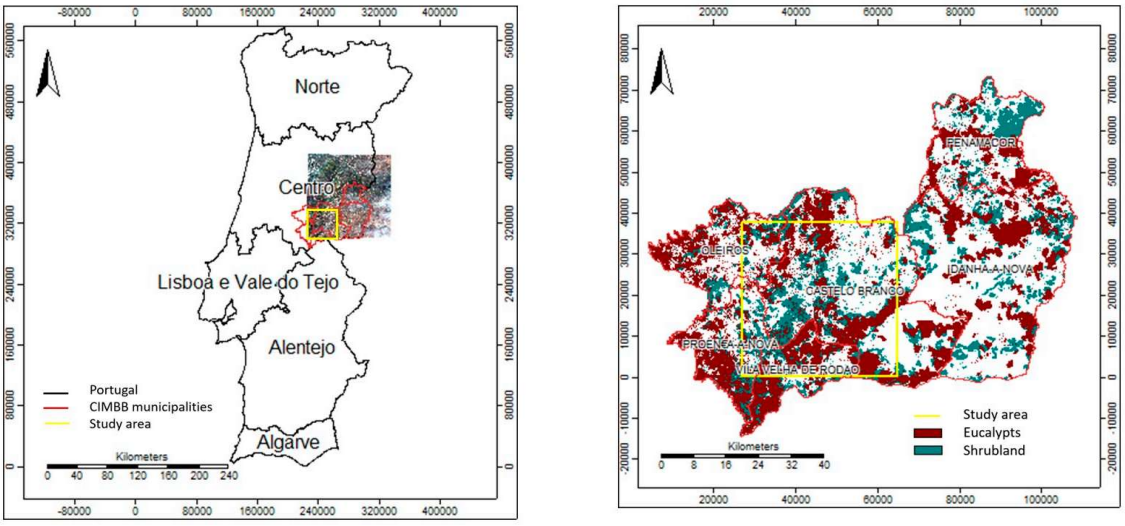

Figure 1. Study area: (**a**) Portugal, the Sentinel2A imagery tile (29 May 2022), the CIMBB municipalities (red) and the study area (yellow); and (**b**) CIMBB's COS 2018 eucalypts areas (brown) and shrubland areas (green).

The latest National Forest Inventory (NFI 2015) statistics indicate that the CIMBB's region was mainly occupied by shrubland and pastures 2,186,890 ha (40.5%) and forests 185,770 ha (40.3%), namely forests of maritime pine 72,540 ha (39.0%) eucalypts 65,240 ha (35.1%), and cork oak 20,900 ha (11.3%) (Figure 1b) [15].

2.2. Data

2.2.1. Land Cover and Land Use Data (COS 2018)

In this study, eucalypts forests cover and shrubland cover maps were extracted from the latest (2018) national reference thematic map for Land Cover and Land Use (LCLU) in Portugal by the Direção Geral do Território (DGT), named as COS (Carta de Ocupação do Solo) (COS2018) [29] (Figure 1b).

The COS2018 map has a scale of 1:25,000, one ha of minimum cartographic unit, a four-level hierarchical classification with 83 classes in the most detailed level [30].

Only pure forests of the species were considered, that is, forests where the dominant species represents more than 75% of the total number of trees and the ground cover is higher than 10%.

Shrubland is defined as natural areas of spontaneous vegetation, little or very dense, in which the shrub cover is greater than or equal to 25% (includes abandoned olive groves if less than 45 trees/ha) [30].

2.2.2. Climatological Data—Local Station (2022)

The climatological station of Castelo Branco is roughly located at the centre of the study area (Figure 1b) and therefore was used to evaluate climatological data regarding the year of 2022. The monthly climatological reports were download from the national official portal of Instituto Português do Mar e da Atmosfera (IPMA) [31] to obtain the evolution of the monthly average temperatures (minimum and maximum, °C) and total monthly precipitation (mm) in the study area (Figure 2).

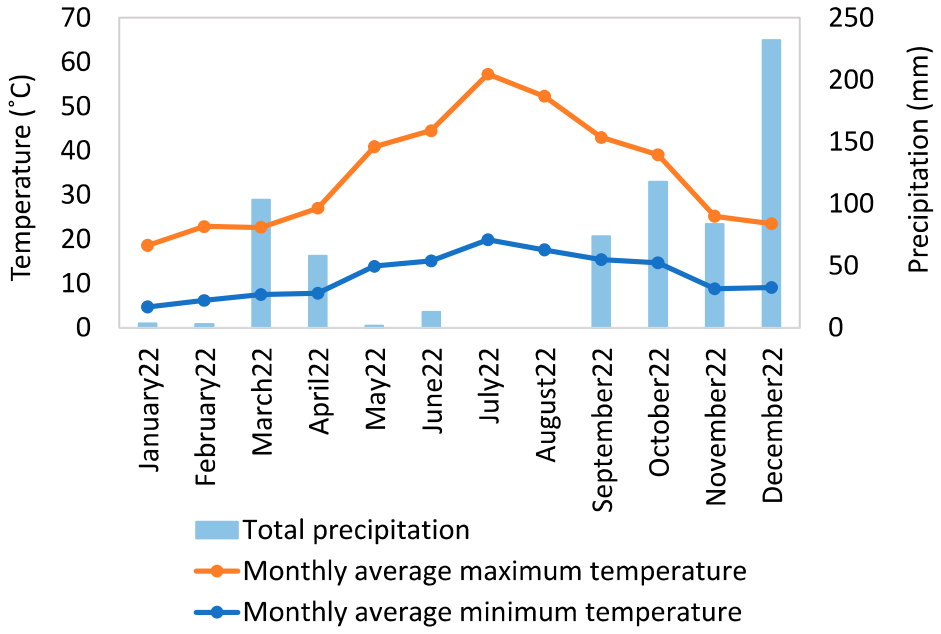

Figure 2. Climatological data: Castelo Branco station (2020–2022)—monthly average temperatures (minimum and maximum, °C) and total monthly precipitation (mm) [31].

2.2.3. Remote Sensing Data—Sentinel2a Imagery

The Sentinel2A imagery data were downloaded from the European Union's earth observation program, called the Copernicus website (https://sentinels.copernicus.eu/web/sentinel/missions/sentinel-2, accessed on 23 June 2023). The Sentinel-2 is one of

the various missions of the Copernicus. Currently, two twin Sentinel-2 satellites (A and B) offer a coverage with high spatial resolution (up to 10 m) and temporal resolution (5 days) [32]. The Sentinel-2 MSI imagery has 13 spectral bands covering the spectral range of 440–2180 nm, with spatial resolutions of 10, 20, and 60 m (Table 1).

Table 1. Sentinel-2 MSI—spectral bands and spatial resolution [26].

Band	Name	Central Wavelength (nm)	Spatial Resolution (m)
1	Coastal aerosol	443	60
2	Blue	490	10 and 20
3	Green	560	10 and 20
4	Red	665	10 and 20
5	Red-edge 1	705	20
6	Red-edge 2	740	20
7	Red-edge 3	783	20
8	NIR	842	10
8a	NIR narrow	865	20
9	Water vapour	945	60
10	Cirrus	1375	60
11	SWIR 1	1610	20
12	SWIR 2	2190	20

In this study, the Sentinel-2 Multispectral Instrument (MSI) imagery, level 2A (atmospherically, radiometrically, and geometrically corrected), was downloaded for 12 monthly dates for the year 2022. The field dates' imagery for June 2023 were also downloaded (Table 2). Regarding the wildfire on 4 August 2023, the pre-fire date (2 August 2023) and post-fire date (12 August 2023) imagery were downloaded as well (Table 2).

Table 2. Sentinel-2A MSI imagery—dates of acquisition.

Year	Date of Acquisition											
	Jan	Feb	Mar	Apr	May	Jun	Jul	Aug	Sep	Oct	Nov	Dec
2022	29	28	30	29	29	28	28	27	26		5 and 25	
2023	4					3, 13, and 23		2 and 12				

2.3. Methods

2.3.1. Sentinel2A Imagery—Vegetation Index NDVI

A Geographical Information System (GIS) software, the free open-source software SAGA 8.5.0 (System for Automated Geoscientific Analyses) (https://saga-gis.sourceforge.io/en/index.html, accessed on 3 February 2023), was used to perform all the computations with the Sentinel2A imagery. The Coordinate System (EPSG 32629): WGS84/UTM zone 29N was used.

The false colour composition and the Normalized Difference Vegetation Index (NDVI—Figure A1) were computed for the 16 dates in 2022 and for the three field dates in 2023 using the spatial resolution of 10 m imagery (Table 3). The Normalized Burn Index (NBR) was computed for the pre-fire and post-fire dates in 2023 using the spatial resolution of 20 m imagery (Table 3).

Table 3. Spectral indices—Normalized Difference Vegetation Index (NDVI) and Normalized Burn Ratio (NBR).

Acronym	Spectral Bands	Formula	Equation
NDVI	R—red band NIR—near infrared band	$\frac{(NIR - R)}{(NIR + R)}$	$\frac{(B8 - B4)}{(B8 + B4)}$
NBR	SWIR—short-wave infrared NIR—near infrared band	$\frac{(NIR - SWIR)}{(NIR + SWIR)}$	$\frac{(B8a - B12)}{(B8a + B12)}$

As it is known, the NDVI values range from −1 to 1, where water surfaces, manmade structures, rocks, clouds, and snow correspond to negative values; bare soil usually falls within the 0.1–0.2 range and plants will always have positive values between 0.2 and 1. Particularly, a healthy, dense vegetation canopy should be above 0.5, and sparse vegetation will most likely fall within the 0.2 to 0.5 range [33].

A grid of 1 km was used to overlay CIMBB's COS 2018 eucalypts layer and shrubland layer (Figure 1b). Regarding the study area, a total of 197 sample points in COS 2018 eucalypts layer (blue) and a total of 227 sample points in shrubland (pink) layer were obtained (Figure 3). The NDVI values computed from the Sentinel-2 imagery for the 12 months in 2022 were extracted for the sample points to obtain the NDVI annual curve for eucalypts and shrubland areas, respectively. The NDVI-CV method by Yang et al. [34] was also applied to differentiate the two types of land cover (eucalypts and shrubland).

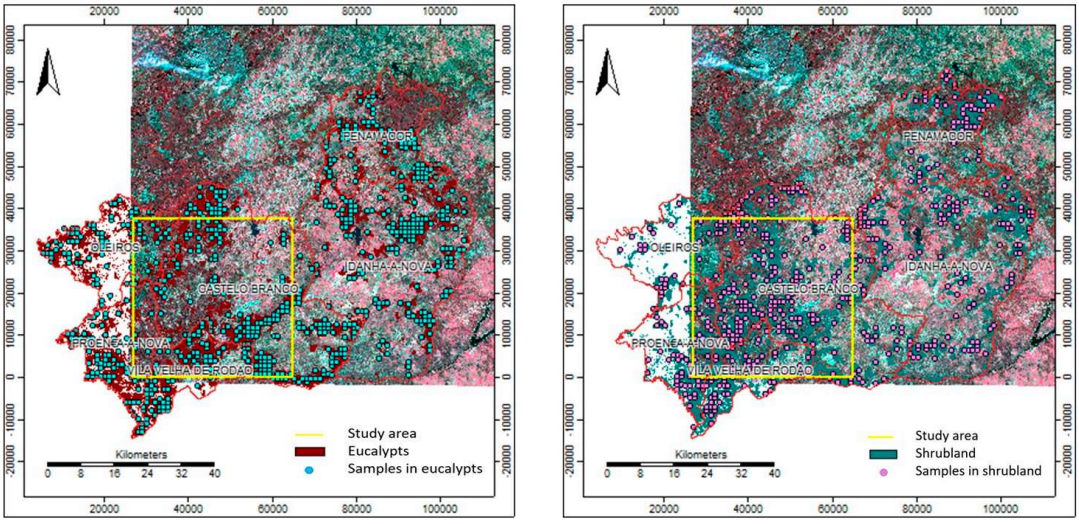

(**a**) (**b**)

Figure 3. Study area—Sentinel2A imagery (29 May 2022) with the sample points: (**a**) in eucalypts areas (blue, n = 197); and (**b**) in shrubland areas (pink, n = 227).

Additionally, the nine spectral bands (e.g., B, G, R, R-edge 1, R-edge 2, R-edge 3, NIR narrow, SWIR 1, and SWIR 2) with a spatial resolution of 20 m for the date of 23 June 2023 were used to extract the correspondent reflectance for the sample points in eucalypts areas and for the sample points in shrubland areas to produce the spectral signatures for these two land covers.

2.3.2. Field Sample Plots—AGB

To collect field data for AGB evaluation, a systematic sampling was applied to the 197 sample points in eucalypts areas (Figure 4a) to select 30 field samples (Figure 4c). Again, a systematic sampling was applied to the 227 sample points in shrubland areas (Figure 4b) and 30 field samples in shrubland areas (Figure 4d). Sample sizes of 30 were considered to

guarantee the minimum amount regarded as statistically significative for data collection due to limited time availability and costs for field data collection. The use of a systematic sampling ensured that the variability of eucalypts and shrubland areas in the study area was covered.

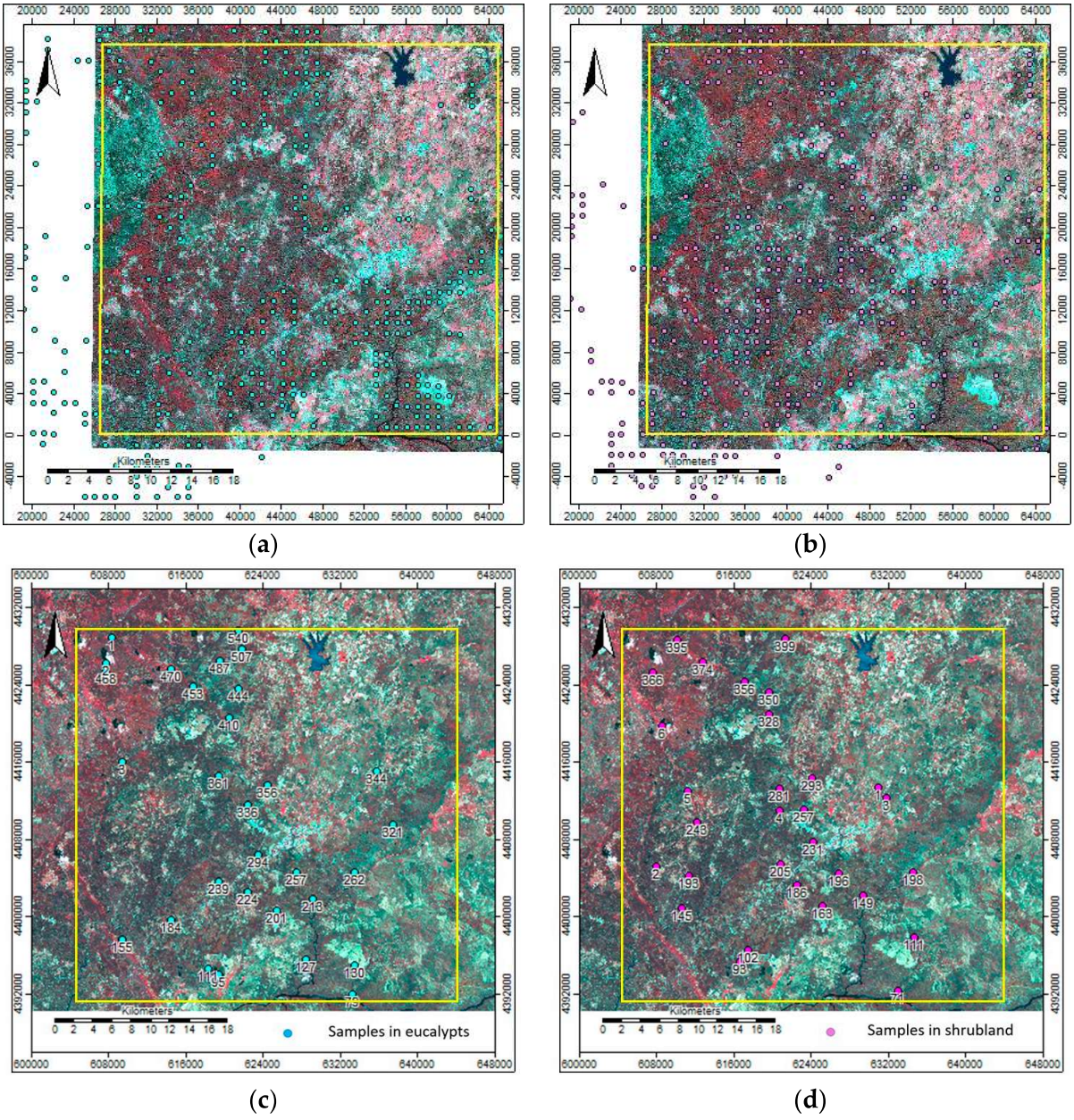

Figure 4. Study area—Sentinel2A imagery (23 June 2023) with the sample points and the field sample plots: (**a**) in eucalypts areas (blue, n = 197); (**b**) in shrubland areas (pink, n = 227); (**c**) in eucalypts areas (blue, n = 30); and (**d**) in shrubland (pink, n = 30).

It should be stressed that, due to the COS2018 map having a minimum cartographic unit of 1 ha, some field sample plots were relocated as they did not fall into the specific land cover under analysis. Therefore, the field sample points' coordinates were updated. Google Earth imagery was used to navigate, locate, and install field sample plots (Figure A2).

Field data were collected between 30 of May and 21 of June 2023. Inventory data in eucalypts areas and in shrubland were collected in circular sample plots with an area of 100 m^2. The diameter at breast height (d in cm) and total height (h in m) were measured in all trees in eucalypts sample plots, using a diameter tape and a hypsometer, respectively.

Afterwards, the following stand variables were evaluated for each sample plot for the characterization of eucalypts stands: age (t), number of trees per ha (N), mean diameter ($\overline{d}$ in cm), mean height ($\overline{h}$ in m), dominant diameter ($ddom$ in cm), and dominant height ($hdom$ in m). Stand dominant diameter and dominant height are defined as the 100 trees of the largest diameter or tallest per hectare, respectively [35]. Thus, in this case, $ddom$ and $hdom$ correspond to the tree of the largest d and to the tree of highest h, respectively. The shrub mean height ($\overline{hs}$ in m) and its ground cover (GC in %) were collected in shrubland sample plots.

To evaluate the AGB of sample plots, the set of models by Tomé et al. [36] for eucalypts in Portugal (Table 4) was used. The set of models was also used by the ICNF to produce the NFI 2015 statistics. Regarding shrubland AGB evaluation, the model by Viana et al. [37] for Portugal was considered (Table 4). This model was fitted with an $R^2 = 0.89$ and used 102 sample plots in the centre–north of Portugal for AGB evaluation using a destructive method.

Table 4. Individual tree biomass prediction equations for eucalypts and shrubland in Portugal [36,37].

Variable	Equation
	Eucalypts
Stem under bark	If $hdom \leq 10.71$ $ws = 0.009964\ d^{\frac{hdom}{-0.70909+0.627861\ hdom}}\ h^{1.369618}$ If $hdom > 10.71$ $ws = 0.009964\ d^{1.780459}\ h^{1.369618}$
Bark	If $hdom \leq 18.2691$ $wb = 0.00594\ d^{\frac{hdom}{-0.69951+0.45855\ hdom}}\ h^{1.084988}$ If $hdom > 18.2691$ $wb = 0.00594\ d^{2.379475}\ h^{1.084988}$
Branches	$wbr = 0.095603\ d^{1.674653}\left(\frac{h}{d}\right)^{-0.85073}$
Leaves	$wl = 0.248952\ d^{1.264033}\left(\frac{h}{d}\right)^{-0.7121}$
Aboveground	$wa = ws + wb + wbr + wl$
	Shrubland
Aboveground	$Was = 0.0258(GC\ hs)^{0.754}$

Legend: $hdom$—stand dominant height (m); d—individual tree diameter, over bark, at breast height (1.30 m above ground) (cm); h—tree total height (m); ws—stem biomass under bark (Kg); wb—bark biomass (Kg); wbr—branch biomass (Kg); wl—leaves biomass (Kg); wa—aboveground biomass (Kg); GC—shrub ground cover (%); hs—shrub average height (cm); and Was—aboveground biomass (Mg ha^{-1}).

2.3.3. AGB Maps Production and Validation

The NDVI was computed from the Sentinel2A imagery available (without clouds) regarding the field data collection period (30 May–21 June 2023). Afterwards, the NDVI values on 3, 13, and 23 June 2023 were extracted for the 30 field sample plots in eucalypts and for the 30 field sample plots in shrubland areas, respectively.

The AGB values evaluated in eucalypts sample plots were modelled with the corresponding NDVI values for the three dates. The same procedure was used regarding the AGB evaluated in shrubland sample plots and the corresponding NDVI values for the three dates. To assess model fitting and prediction performances, the following statistics were considered: the coefficient of determination (R^2); model bias, evaluated with the mean prediction errors (e); model precision, with the mean of the absolute value of the prediction errors (ae) and the prediction error variance (σ^2e); and the modelling efficiency (R^2e), a measure equivalent to the coefficient of determination but computed with the prediction errors [38].

The NDVI imagery was used as input to compute the AGB for eucalypts and shrubland by using the respective fitted models Wa = f(NDVI). Afterwards, the COS2018 regarding

eucalypts and shrubland areas were used to clip the AGB in those specific areas. For validation purposes, the AGB values were extracted for the 30 field sample points in eucalypts and the 30 field sample points in shrubland areas. Finally, the AGB values were also extracted for eucalypts and shrubland areas and compared to other data sources.

Finally, the wildfire on 4 August 2023 was used to compare fuel loads and burn severity levels. This fire burn scar was obtained using the NBR computed from the Sentinel2A imagery (spatial resolution of 20 m) of the pre-fire date (2 August 2023) and post-fire date (12 August 2023). Then, the difference of the NBR between the two dates was obtained. Afterwards, the dNBR was used to classify burn severity according to the levels proposed by EFFIS (Table 5) [26].

Table 5. Burn severity—differenced Normalized Burn Ratio (dNBR) thresholds proposed by the European Forest Fire Information Service (EFFIS) [26].

EFFIS Thresholds	Severity Levels
dNBR < 0.100	Unburned/Very low
0.100 ≤ dNBR ≤ 0.255	Low
0.256 ≤ dNBR ≤ 0.419	Moderate
0.420 ≤ dNBR ≤ 0.660	High
dNBR > 0.660	Very high

3. Results

3.1. NDVI Annual Curve (2022)

The values extracted from the NDVI imagery for 2022 (Figure A1) regarding the sample points (Figure 5; eucalypts areas n = 197 and shrubland areas n = 227) and the field sample points in eucalypts areas and in shrubland areas (n = 30 for eucalypts and shrubland areas, respectively) are summarized in Table 6.

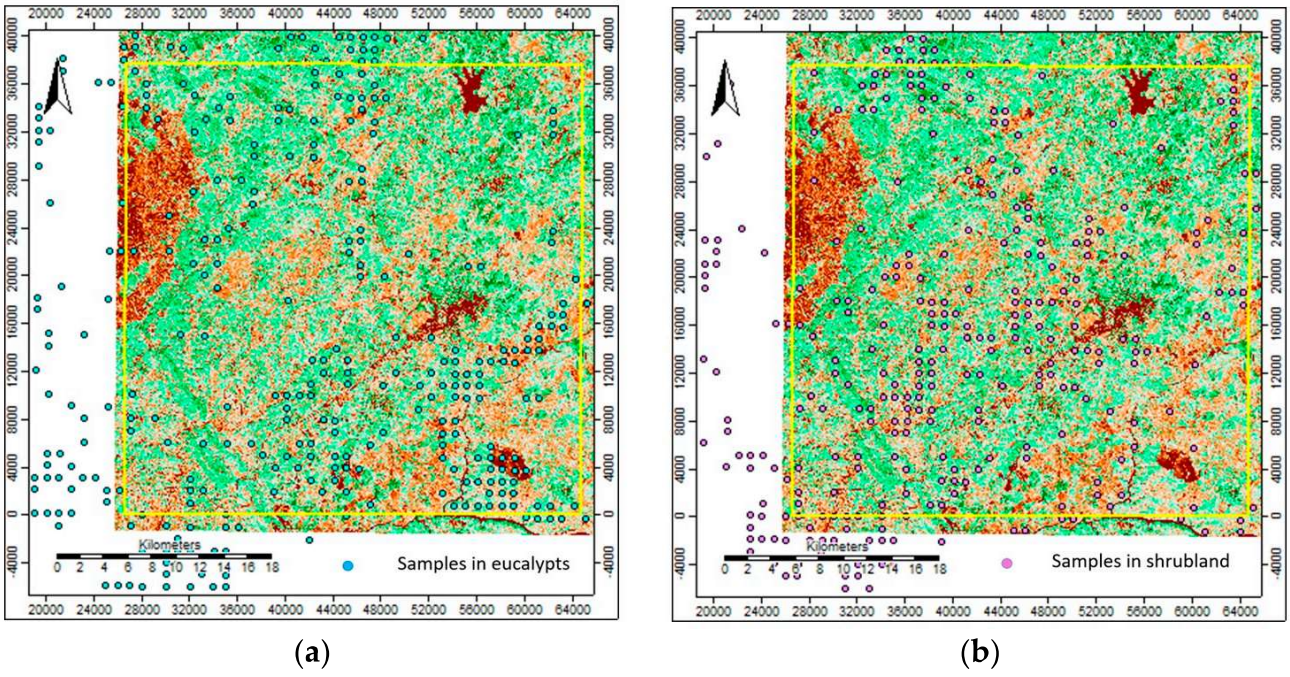

Figure 5. Study area—NDVI imagery (29 May 2022) with the sample points: (**a**) in eucalypts areas (blue, n = 197); and (**b**) in shrubland areas (pink, n = 227).

Table 6. NDVI—summary statistics: sample points in eucalypts areas (n = 197) and in shrubland areas (n = 227); and field sample points in eucalypts areas (n = 30) and in shrubland areas (n = 30).

NDVI	Eucalypts Areas (n = 197)				Shrubland Areas (n = 227)				Eucalypts Areas (n = 30)				Shrubland Areas (n = 30)			
Date	Min.	Max.	Mean	SD	Min.	Max.	Mean	SD	Min.	Max.	Mean	SD	Min.	Max.	Mean	SD
29 Jan 22	0.098	0.517	0.339	0.082	0.131	0.488	0.315	0.065	0.186	0.507	0.371	0.067	0.253	0.442	0.350	0.052
28 Feb 22	0.072	0.459	0.311	0.077	0.103	0.479	0.303	0.061	0.090	0.435	0.329	0.075	0.230	0.412	0.328	0.045
30 Mar 22	0.069	0.433	0.285	0.062	0.066	0.425	0.289	0.053	0.033	0.403	0.296	0.074	0.207	0.366	0.306	0.036
29 Apr 22	0.086	0.478	0.280	0.059	0.116	0.440	0.296	0.051	0.197	0.443	0.296	0.057	0.213	0.385	0.299	0.040
29 May 22	0.061	0.531	0.279	0.079	0.103	0.546	0.296	0.080	0.158	0.408	0.279	0.061	0.172	0.409	0.284	0.061
28 Jun 22	0.061	0.478	0.265	0.075	0.091	0.500	0.271	0.080	0.141	0.372	0.263	0.060	0.119	0.372	0.269	0.066
28 Jul 22	0.043	0.446	0.253	0.079	0.063	0.492	0.243	0.082	0.115	0.391	0.253	0.068	0.103	0.364	0.254	0.070
27 Aug 22	0.062	0.447	0.257	0.075	0.075	0.476	0.237	0.074	0.133	0.383	0.259	0.064	0.114	0.364	0.255	0.067
26 Sep 22	0.066	0.467	0.291	0.082	0.071	0.491	0.276	0.080	0.148	0.417	0.303	0.072	0.120	0.390	0.286	0.077
5 Nov 22	0.082	0.495	0.340	0.083	0.128	0.482	0.310	0.068	0.151	0.455	0.358	0.079	0.214	0.424	0.335	0.066
25 Nov 22	0.097	0.511	0.350	0.077	0.133	0.479	0.321	0.067	0.170	0.508	0.372	0.073	0.262	0.482	0.362	0.059
4 Jan 23	0.100	0.521	0.357	0.079	0.134	0.516	0.317	0.069	0.260	0.529	0.389	0.060	0.285	0.481	0.370	0.054

Legend: n—sample size; Min.—minimum; Max.—maximum; SD—standard deviation.

The analysis of the average monthly NDVI values for 2022 for the sample points and the field sample points in eucalypts areas and in shrubland areas (Table 6; Figure 6a) showed that the values in the field sample points are slightly higher (Figure 6a; E_ and S_) compared to the sample plots (Figure 6a; E and S). This may be explained by the validation of the field sample points by ground truth, corresponding to that specific land cover. Conversely, due to the COS2018's minimum cartographic unit of 1 ha, some sample points may have been classified as belonging to that land cover class, but "in loco" is a different land cover that was aggregated to the dominant class, resulting in some "noise" as the NDVI imagery spatial resolution is of 10 m × 10 m (0.01 ha).

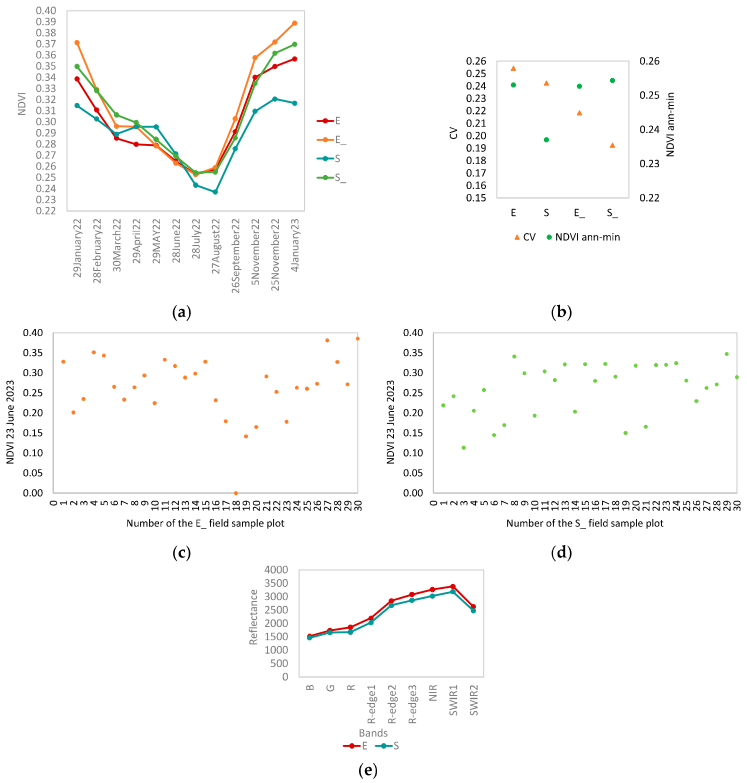

Figure 6. Study area—sample points and field sample points for eucalypts and shrubland areas (E, n = 197; S, n = 227; E_, n = 30; S_, n = 30): (**a**) NDVI annual curve (2022); and (**b**) NDVI-CV method (2022); (**c**) eucalypts field sample plots NDVI on 23 June 2023; (**d**) shrubland field sample plots NDVI on 23 June 2023; and (**e**) spectral signatures (23 June 2023).

Overall, the minimum annual NDVI was observed between July and August in accordance with the climatological data (Figure 2). The NDVI-CV method allowed differentiating eucalypts from shrubland areas (Figure 6b). Field sample points showed a lower coefficient of variation (CV; %) and higher NDVI annual minimum (Figure 6b; E_ and S_). In eucalypts field plots (Figure 6c), the minimum NDVI value was observed in a recent plantation (N = 2900 trees ha^{-1}; *ddom* = 6.5 cm) with a great portion of bare soil. Conversely, the maximum NDVI value was observed in mature eucalypts (N = 1000 trees ha^{-1}; *ddom* = 24 cm). Regarding shrubland field plots (Figure 6d), the minimum and maximum NDVI values were not related to the ground cover or the average height, but to a combined effect of those variables, the species present, and their distribution over the sample plot. The signature curves also showed a differentiation between the two types of land cover, particularly on the NIR band (Figure 6e).

3.2. AGB Maps Production and Validation

The AGB estimated from the 30 field sample plots in eucalypts areas and 30 sample field sample plots in shrubland areas (Table 7) showed, for eucalypts areas, an average AGB of 78.7 Mg ha^{-1}, and for shrubland areas, an average AGB of 107.3 Mg ha^{-1}.

Table 7. Forest inventory—summary statistics for field sample plots in eucalypts areas (n = 30) and in shrubland areas (n = 30).

Variables		Min.	Max.	Mean	SD
		Eucalypts field sample plots (n = 30)			
Number of trees per ha	N (trees ha^{-1})	800	4500	1923	799
Mean diameter	$\overline{d}$ (cm)	3.5	20.6	9.1	3.2
Mean height	$\overline{h}$ (m)	6.6	19.2	12.6	3.3
Dominant diameter	*ddom* (cm)	6.0	26.6	14.1	4.8
Dominant height	*hdom* (m)	10.0	25.0	16.5	4.5
Aboveground biomass	*Wa* (Mg ha^{-1})	27.7	169.0	78.7	35.0
		Shrubland field sample plots (n = 30)			
Ground cover	*GC* (%)	10.0	90.0	43.0	20.9
Shrub average height	$\overline{hs}$ (m)	50.0	180.0	117.7	36.5
Aboveground biomass	*Was* (Mg ha^{-1})	2.8	33.6	16.4	8.3

Legend: n—sample size; Min.—minimum; Max.—maximum; SD—standard deviation.

Eucalypts field sample plots offered a good coverage of the stands' variability of age classes. Regarding shrubland areas, the dominant species observed in the field were: gum rockrose, lavender, brooms, heather, and gorse flower tea (*Cistus ladanifer*; *Lavandula* spp.; *Cytisus* spp., *Genista* spp. or *Spartium* spp.; *Erica* spp. or *Calluna* spp.; and *Pterospartum tridentatum*, respectively) (Figure 7).

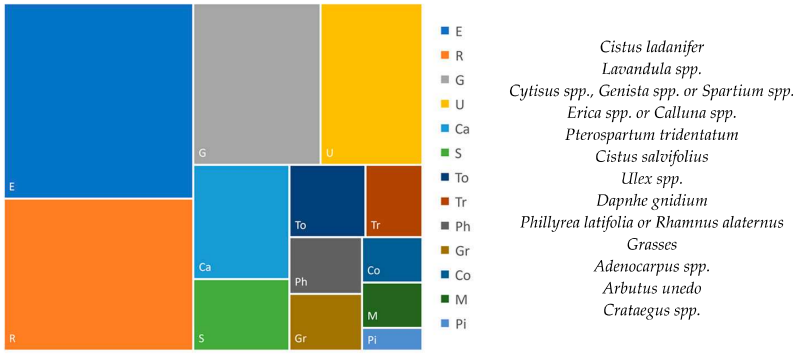

Figure 7. Study area—shrubland areas' species composition.

The analysis of the NDVI values for the three field dates in 2023 extracted for the 30 sample field sample plots in eucalypts areas and 30 sample field sample plots in shrubland areas (Figure 8) are summarized in Table 8.

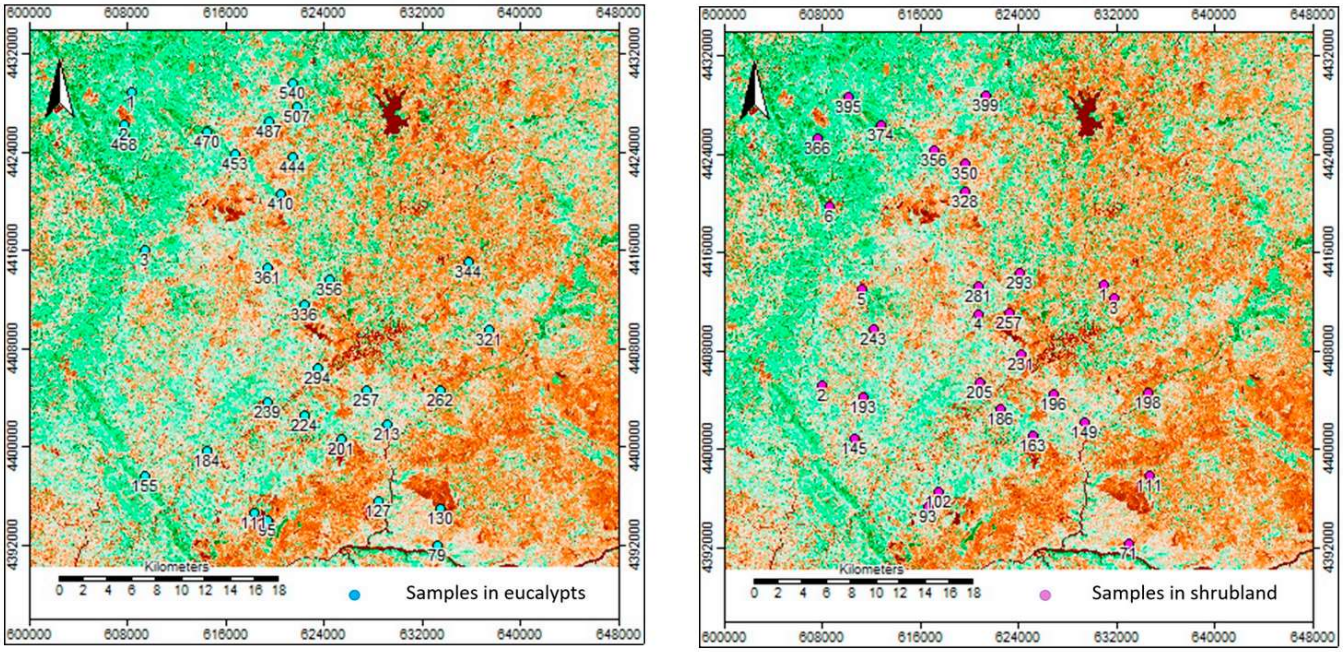

(**a**) (**b**)

Figure 8. Study area—NDVI imagery (23 June 2023) with the field sample plots: (**a**) in eucalypts areas (blue, n = 30); and (**b**) in shrubland (pink, n = 30).

Table 8. NDVI—summary statistics for the field sample plots in eucalypts areas (n = 30) and in shrubland areas (n = 30).

NDVI	Eucalypts Field Sample Plots (n = 30)				Shrubland Field Sample Plots (n = 30)			
Date	**Min.**	**Max.**	**Mean**	**SD**	**Min.**	**Max.**	**Mean**	**SD**
3 Jun 23	0.000	0.344	0.192	0.098	0.043	0.369	0.219	0.101
13 Jun 23	0.000	0.437	0.243	0.110	0.006	0.372	0.227	0.105
23 Jun 23	0.000	0.386	0.264	0.079	0.114	0.348	0.260	0.065

Legend: n—sample size; Min.—minimum; Max.—maximum; SD—standard deviation.

A linear correlation between the estimated AGB in the field sample plots and the correspondent NDVI values extracted for the plots was obtained with the best fitting efficiency on 23 June 2023 for both eucalypts plots (R^2 = 0.76; Figure 9a) and shrubland plots (R^2 = 0.77; Figure 9b). Prediction statistics for eucalypts AGB estimation (*Wa* predicted) showed a bias of 5.99 Mg ha^{-1} and a precision of 35.47 Mg ha^{-1} (Figure 9c). Regarding prediction statistics for shrubland AGB estimation (*Was* predicted), a bias of 0.87 Mg ha^{-1} and a precision of 7.29 Mg ha^{-1} were obtained (Figure 9d).

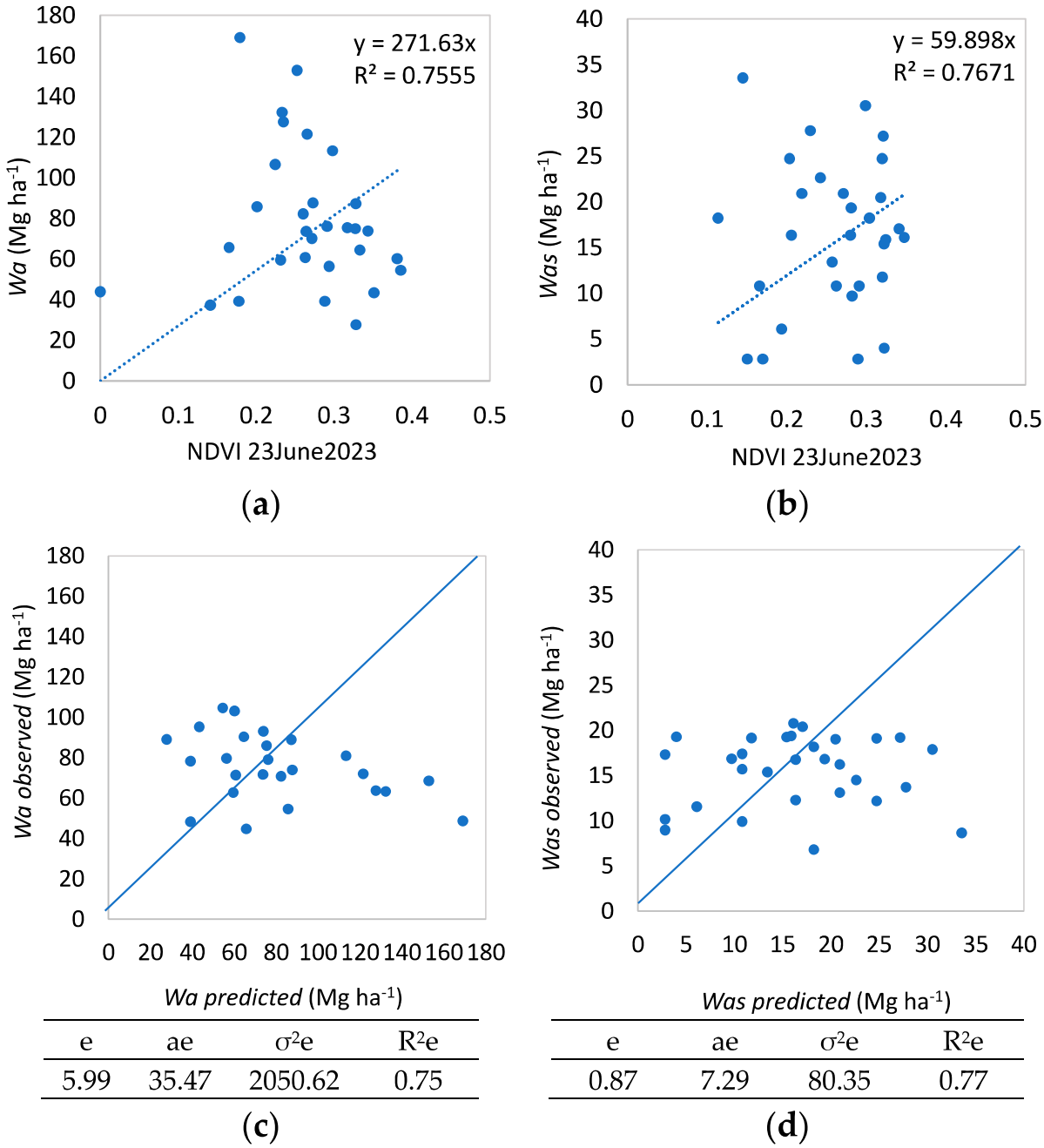

e	ae	σ²e	R²e
5.99	35.47	2050.62	0.75

e	ae	σ²e	R²e
0.87	7.29	80.35	0.77

Figure 9. Study area—modelling and validation: (**a**) Wa = f(NDVI) for eucalypts plots; (**b**) Wa = f(NDVI) for shrubland plots; (**c**) prediction residuals for eucalypts plots; and (**d**) prediction residuals for shrubland plots. **Legend**: R^2—model coefficient of determination; e—model bias; ae—model precision; σ^2e—prediction error variance; and R^2e—modelling efficiency.

The COS2018 regarding eucalypts areas and shrubland areas and the corresponding AGB maps are presented in Figure 10. The AGB values extracted for eucalypts areas presented an average of 78.76 Mg ha^{-1}, and for shrubland areas, an average of 15.55 Mg ha^{-1} (Table 9), which were thus consistent with the average estimated field values (Table 7).

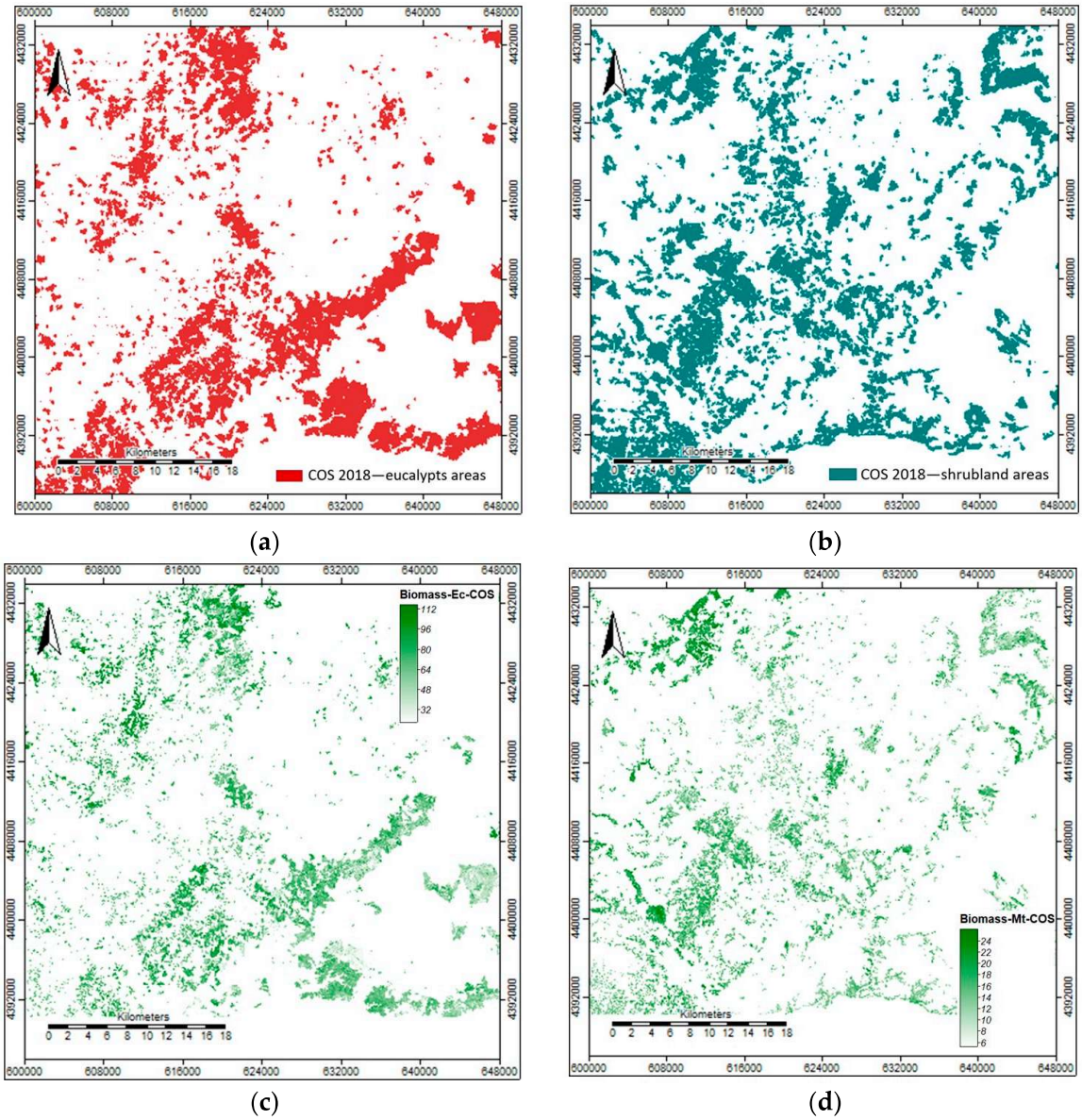

Figure 10. Study area: (**a**) COS 2018—eucalypts areas; (**b**) COS 2018—shrubland areas; (**c**) AGB—eucalypts areas; and (**d**) AGB—shrubland areas.

Table 9. AGB—summary statistics in eucalypts areas (n = 2773 polygons) and in shrubland areas (n = 2905 polygons).

AGB		Min.	Max.	Mean	SD
Eucalypts areas	*Wa* (Mg ha^{-1})	16.31	141.82	78.76	15.85
Shrubland areas	*Was* (Mg ha^{-1})	6.81	20.82	15.55	3.92

Legend: n—sample size; Min.—minimum; Max.—maximum; SD—standard deviation.

A detailed insight of the AGB maps' outputs is shown using zoom areas with eucalypts (Figure 11) and with shrubland (Figure 12), wherein the AGB maps' outputs are overlayed with the FCC and NDVI imagery. The AGB maps showed a good consistency with the observed detail in the FCC and NDVI imagery.

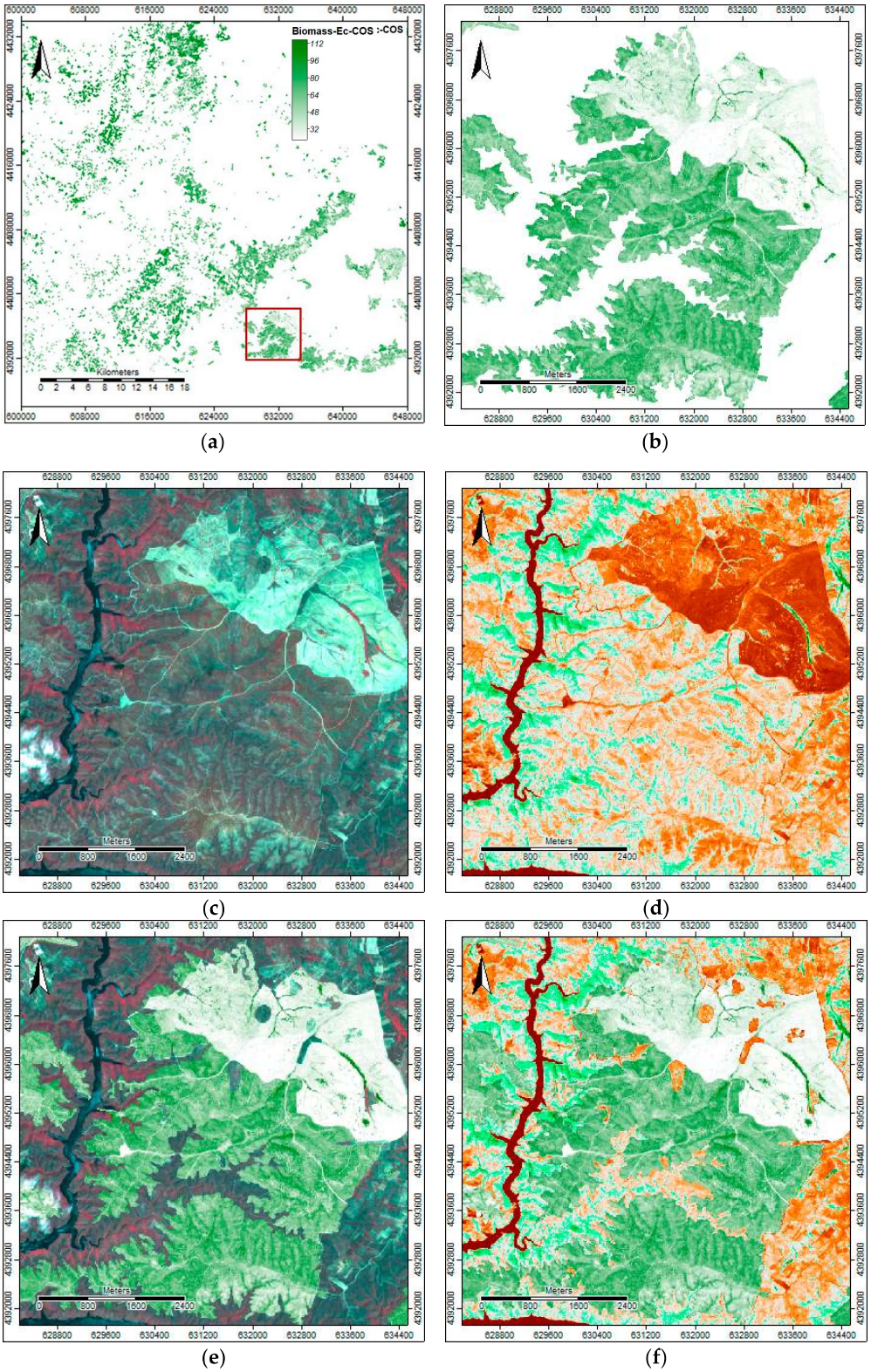

Figure 11. Study area: (**a**) Eucalypts AGB map; (**b**) AGB map—zoom; (**c**) FCC—zoom; (**d**) NDVI—zoom; (**e**) AGB overlay FCC—zoom; (**f**) AGB overlay NDVI—zoom.

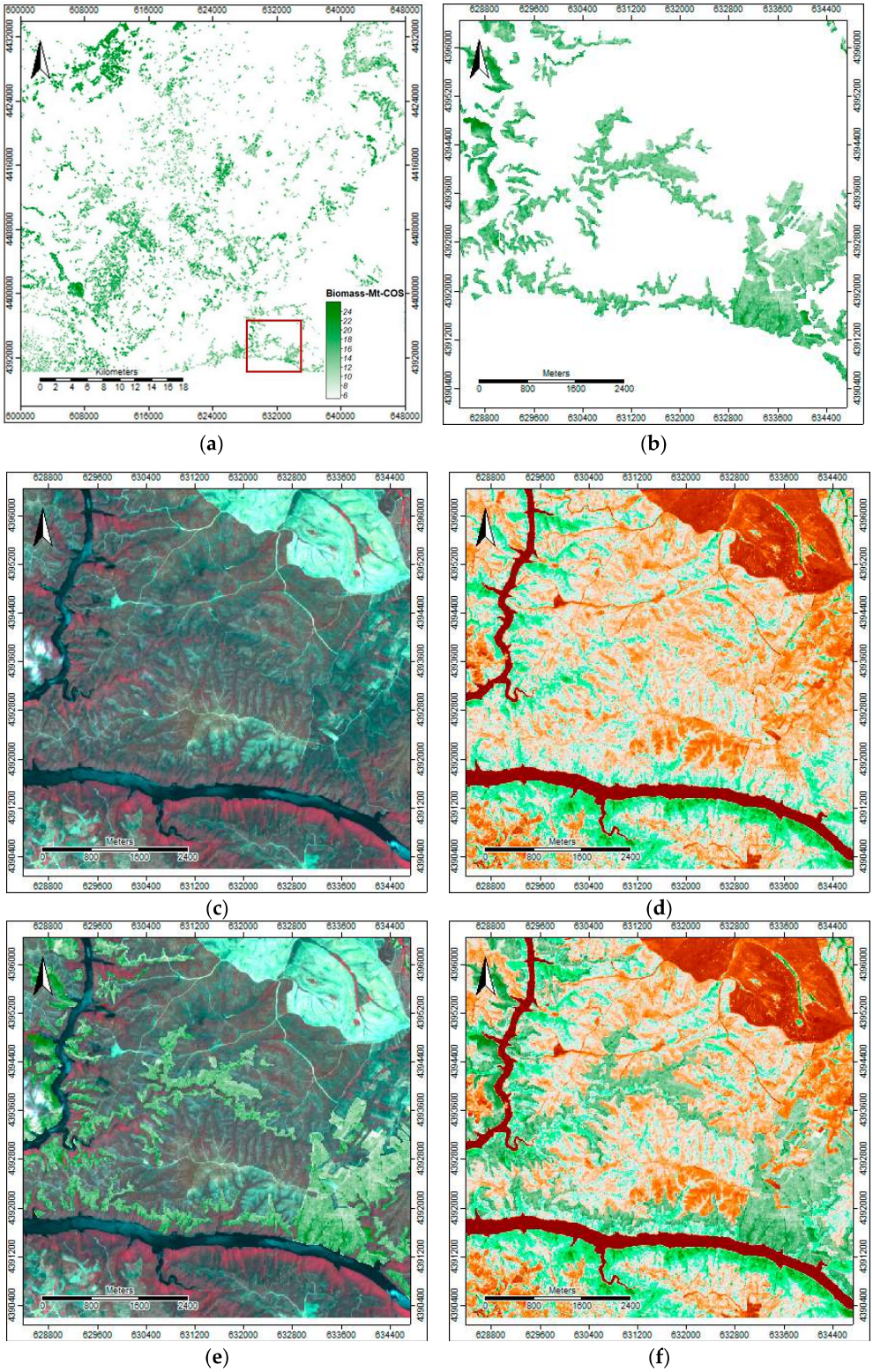

Figure 12. Study area: (**a**) Shrubland AGB map; (**b**) AGB map—zoom; (**c**) FCC—zoom; (**d**) NDVI—zoom; (**e**) AGB overlay FCC—zoom; (**f**) AGB overlay NDVI—zoom.

Finally, a joint map of AGB for both eucalypts and shrubland areas provided an overall perspective of fuel loads throughout the study area (Figure 13). Higher loads were observed at the left side compared to the right side (Figure 13a), which are mountainous areas (Figure 13b) wherein slope and fuel loads have a multiplicative increasing effect on fire potential severity evaluation. The wildfire on 4 August 2023 started at 15:03 h and,

due to the wind, evolved and progressed towards the southeastern direction, climbing the mountain named Serra das Tapadas, towards the adjacent municipality of Proença-a-Nova (Figure 13c). High burn severity levels were observed in Serra das Tapadas' burn area (Figure 13d), wherein significative fuel loads were available (Figure 13c).

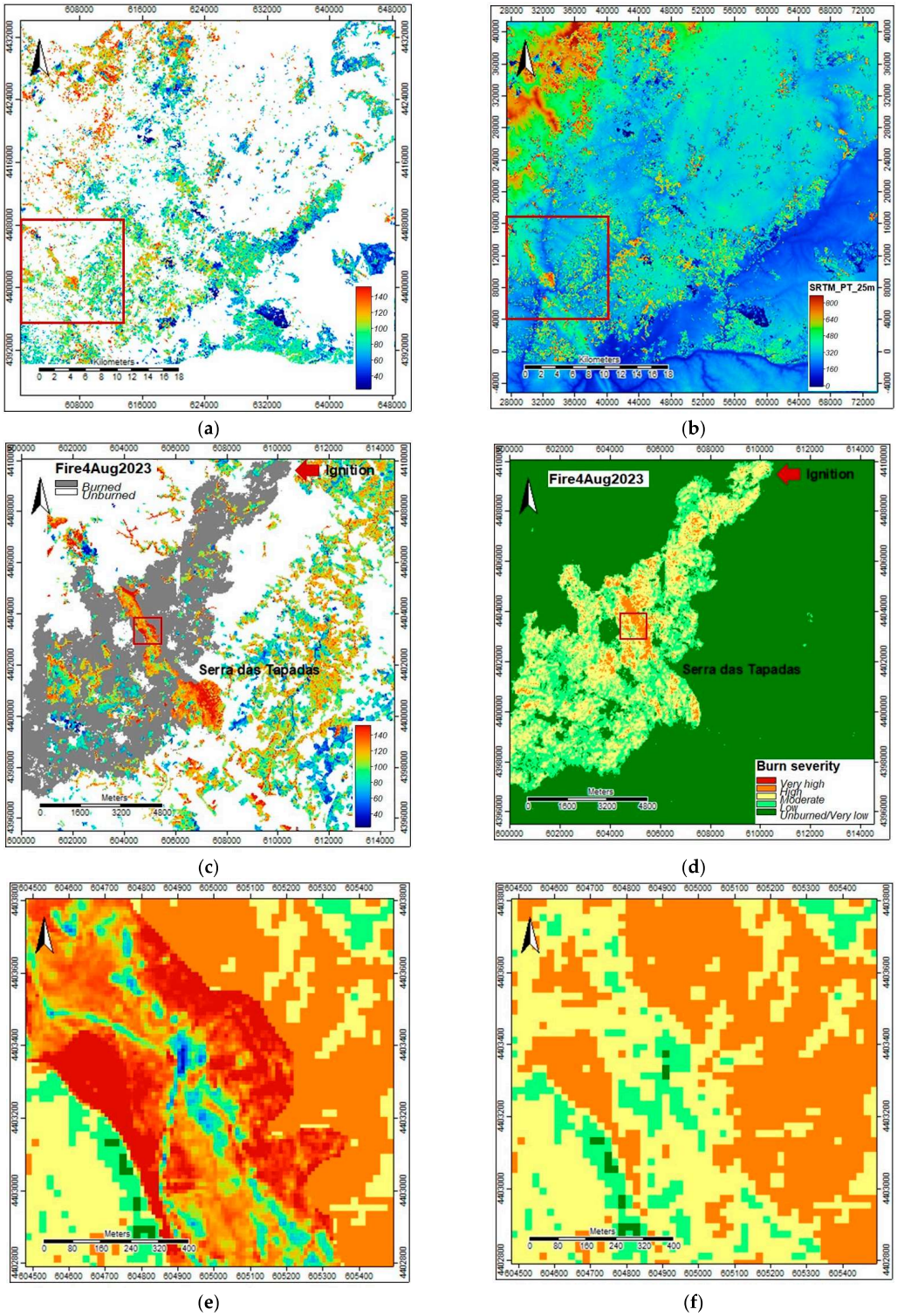

Figure 13. Study area—fuel loads: (**a**) AGB—eucalypts and shrubland areas; (**b**) AGB map overlaid to the elevation map (25 m spatial resolution) [39]; (**c**) wildfire on 4 August 2023—burned area and fuel loads; (**d**) wildfire on 4 August 2023—burn severity levels by EFFIS; (**e**) zoom—burned area and fuel loads; and (**f**) zoom—burn severity levels by EFFIS.

4. Discussion

Our research hypothesis was that the NDVI is a reliable predictor for mapping AGB in eucalypts and shrubland areas to provide a decision support tool for forest management and for mitigating fire hazard and fire severity. Firstly, the NDVI time curve for 2022 showed a minimum observed between July and August for both eucalypts and shrubland areas, which was in accordance with the climatological data for that same year. The NDVI-CV allowed differentiating eucalypts from shrubland areas. The spectral signature curves also showed a differentiation between the two types of land cover, particularly on the NIR band. These results are consistent with the theoretical knowledge that broadleaved forests (e.g., eucalypts) have high NIR reflectance, thus consequently higher NDVI values than other types of vegetation [40]. Some studies also confirm this result when comparing coniferous (e.g., maritime pine) and broadleaved (e.g., eucalypts) forests [34,41]. Some observed inversions throughout the NDVI time curve may be explained by the species phenology such as the flowering season, particularly concerning shrubs species. In young eucalypts plantations, low NDVI values should also be considered, as at the plantation stage, substantial bare soil is exposed (spatial resolution 10 × 10 m). Indeed, in a recent plantation (N = 2900 trees ha^{-1}; *ddom* = 6.5 cm), the corresponding NDVI value was zero. Conversely, in a mature eucalypt plantation (N = 1000 trees ha^{-1}; *ddom* = 24 cm), the maximum NDVI value of 0.39 was observed. In fact, the NDVI measures vegetation greenness in relation to vegetation productivity. Thus, stand variables such as age, density, and tree dimensions also need to be taken into consideration when explaining NDVI values. Regarding shrubland NDVI values, an obvious relation to the ground cover or to the average height was not found. Thus, differences in NDVI values may be explained as a combined effect of those variables, the species present, and their distribution over the sample plot. To better understand the impact of the type of species and its distribution, it would be necessary to collect more detailed field information (e.g., the ground cover and the average height by species along several transepts in the field sample plot).

Nevertheless, in this study, the NDVI values for eucalypts and shrubland areas were found to be smaller than the ones obtained in a previous study [41]. For instance, the following NDVI values were observed: mature eucalypts plantations (NDVI = 0.82), young eucalypts plantations (NDVI = 0.56), strawberry tree shrubland (NDVI = 0.56), eucalypts plantations post-fire (NDVI = 0.49), tall shrubland (NDVI = 0.46), and short shrubland (NDVI = 0.44). These differences may be explained by eucalyptus productivity in this study area, with a less dry climate, and by the composition of the existent shrubs' species (e.g., *Arbutus unedo*, *Erica* sp., and *Cytisus* sp.). Indeed, it is well known that temperature and precipitation as related variables have a determinant role in species distribution and productivity [42].

Secondly, it should be stressed that the circular plots with an area of 100 m^2 for field data collection matched the spatial resolution of the NDVI imagery computed from the Sentinel2A imagery (cell size 10 × 10 m), which provided a perfect correspondence between field estimates and the computed NDVI values. Moreover, the Sentinel2A imagery date used to compute the NDVI had no clouds and was very close to the field dates. Despite the fact that the sample size (n = 30) used in this study proved to have been statistically significant, it would have been beneficial to have a more robust dataset for AGB modelling. Nevertheless, this study's AGB estimates will provide a base for planning future field work and help set the adequate number of samples under a required precision level.

Thirdly, it was proven that the NDVI imagery computed from the Sentinel2A imagery with a spatial resolution of 10 m was found to be a reliable predictor for mapping AGB in eucalypts and shrubland areas for the study area. Indeed, the fitted linear models for AGB prediction using the NDVI imagery showed good fitting performances (R^2 of 0.76 and 0.77, respectively). The results obtained in this study are consistent with other studies, for other species and regions, where biomass maps were produced using allometric equations of NDVI that were computed from a variety of satellite imagery (e.g., SPOT-6, Indian Remote Sensing Satellite (IRS-ID) LISS III, and Sentinel2) and similar fitting performances (R^2 from

0.56 to 0.89%) were achieved [2,3,5,6,10,41,43,44]. Regarding AGB estimation accuracy, the prediction statistics for eucalypts showed a bias of 5.99 Mg ha^{-1} and a precision of 35.47 Mg ha^{-1}, and for shrubland, a bias of 0.87 Mg ha^{-1} and a precision of 7.29 Mg ha^{-1} was obtained. However, an improvement on the accuracy of these estimates may be expected if regional biomass models applicable to this study area are available. Indeed, the eucalypts biomass models used in this study were fitted for Portugal and the shrubland biomass model was fitted for the centre–north of Portugal.

According to the NFI 2015 statistics, eucalypts areas in CIMBB represented a biomass of 1654 Mg in live trees (aboveground and roots) (3032 Mg CO_{2e}) [15]. In this study, field data estimation resulted in an average AGB of 78.7 Mg ha^{-1} in eucalypts areas and an average AGB of 15.55 Mg ha^{-1} in shrubland areas. The AGB maps provided an average estimation for AGB production of 78.8 Mg ha^{-1} in eucalypts areas and an average AGB production of 15.55 Mg ha^{-1} in shrubland areas, which were therefore very consistent with the field estimates. The result for eucalypts is consistent with a study performed in this region, where an average AGB production between 52.0 and 75.8 Mg ha^{-1} at the harvest age was obtained (e.g., three 14-year coppices) [18]. Overall, bark and leaves biomass represented 18% of the AGB and were recommended to be retained at the felling site after harvest/commercial thinning to mitigate the update of soil nutrients [18]. The results for shrubland areas are also consistent with the AGB evaluation in the centre–north of Portugal by Viana et al. [37].

The eucalypts AGB map can be very useful to support this species management and to forecast its environmental impact. Both eucalypts and shrubland AGB maps can be critical to support fuel load management in these areas to mitigate fire hazard and fire severity. As the species, stand variables (e.g., stand density and stand height), and topographic variables (e.g., slope and aspect) of contiguous patches can be used to predict fire severity [23], the AGB maps can also provide a valuable input regarding fire potential severity assessment.

In Portugal, fire hazard maps are produced at the municipality level based on the latest LCLU (COS 2018), and so, incorporating updated information would be beneficial. The fire hazard map is based on a multiplicative spatial model of the following raster layers: (1) annual fire probability and (2) fire susceptibility [25]. The fire susceptibility map is produced by multiplying the layers' slopes and LCLU after being reclassified into classes of increasing susceptibility [25]. For instance, adding a multiplicative layer of fuel loads, reclassified as well by increasing susceptibility classes, may improve the fire susceptibility map. Indeed, the occurrence of a wildfire on 4 August 2023 at the southeastern side of the study area provided the opportunity to compare fuel loads and the burn severity levels by EFFIS assessed for that burn area. The burn severity map identified high burn severity levels in the mountainous burn area, wherein the fuel load map had anticipated high fuel loads, proving the importance of this type of information to support decision-making on civil protection. Thus, updated information about fuel loads obtained by the AGB maps computed from the most recent Sentinel2A imagery will provide key information for decision-making. Hence, future research is crucial for producing AGB maps for other forest species, particularly for maritime pine due to its high proneness to fire.

Overall, fire potential can be forecasted according to the type of fire behaviour based on the terrain topography (e.g., type, slope, and aspect), the fuel types associated to the land cover present in the area, and the weather. But, when a wind shift is forecasted at a predicted time, the conditions and impact of this wind shift on fire behaviour are uncertain. Thus, detecting sources of uncertainty in fire management scenarios should unquestionably be a part of the decision-making process. Thus, collaborative science is fundamental to provide clear solutions to support the decision-making process on civil protection to avoid the collapse in its capacity when resolving extreme wildfires [45].

5. Conclusions

This study proved the possibility of producing AGB maps for eucalypts and shrubland areas by using the NDVI imagery as the sole predictor with good fitting and prediction

performances. Nevertheless, further research is needed to obtain regional biomass models and to obtain more robust datasets for the independent validation of the models.

The AGB maps provide a relevant decision support tool for forest management and for fire hazard and fire severity mitigation. The AGB maps deliver updated information of field fuel loads as they are estimated using the NDVI, computed from the most recent Sentinel2A imagery. Yet, this study focused only on AGB mapping for eucalypts and shrubland areas. Thus, future research is crucial on producing AGB maps for other forest species, particularly for maritime pine due to its high proneness to fire.

Furthermore, the AGB maps can be integrated in the Portuguese fire hazard model to obtain a more reliable and updated fire severity assessment in near real-time by using Sentinel2A imagery. Finally, in a wildfire scenario, estimating current field fuel loads provide intelligent information to support decision-making on civil protection.

Funding: This study was funded by CERNAS-IPCB [UIDB/00681/2020], funding from the Foundation for Science and Technology (Fundação para a Ciência e Tecnologia—FCT).

Data Availability Statement: Not applicable.

Acknowledgments: To Carlos Grácio and Natália Roque, our colleagues at the Polytechnic University/Instituto Politécnico de Castelo Branco (IPCB), for technical support regarding the field data collection. To the students Thais Ismael and Ângelo Semedo for field data collection under our supervision and for their thesis in Renewable Energy Engineering Graduation course of the IPCB.

Conflicts of Interest: The author declares no conflict of interest. The funders had no role in the design of the study.

Appendix A

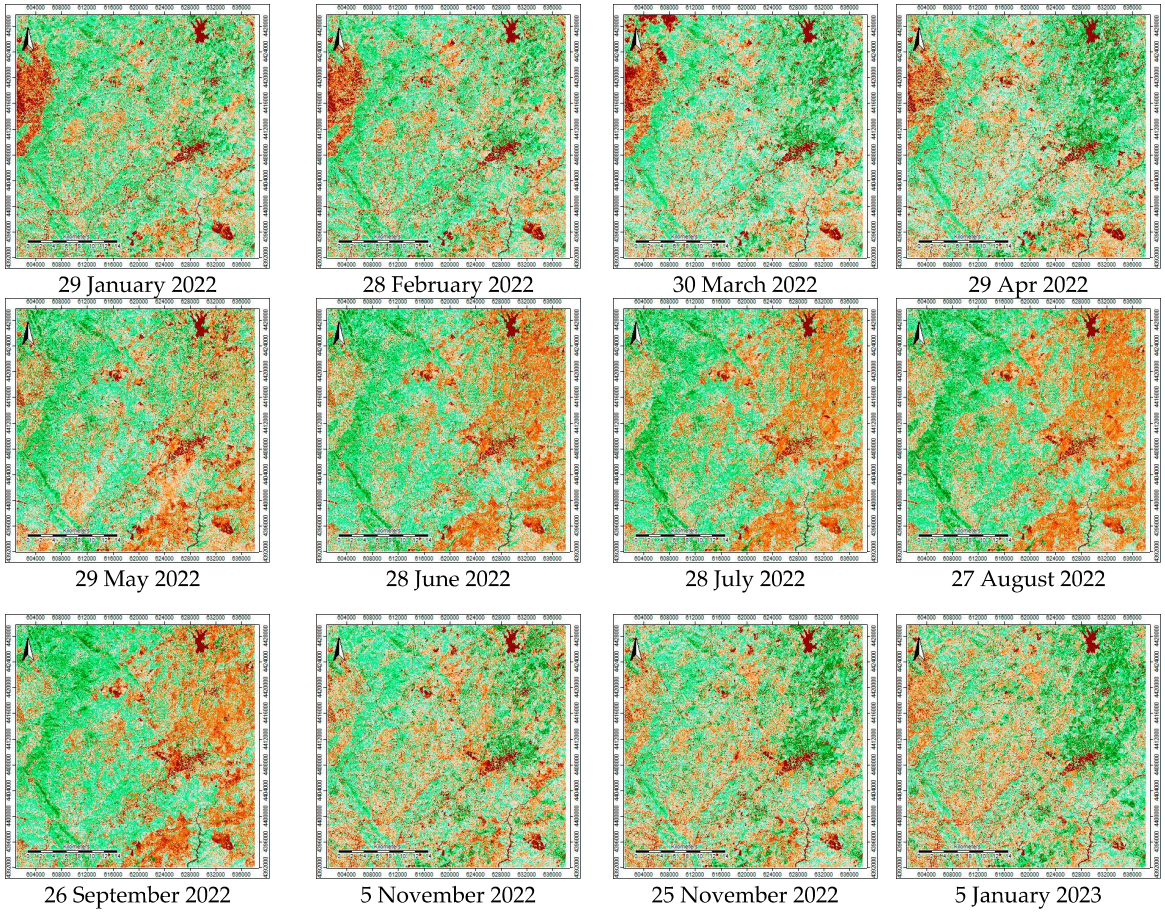

Figure A1. Study area—Sentinel2A imagery clip: NDVI imagery (January 2022 to January 2023).

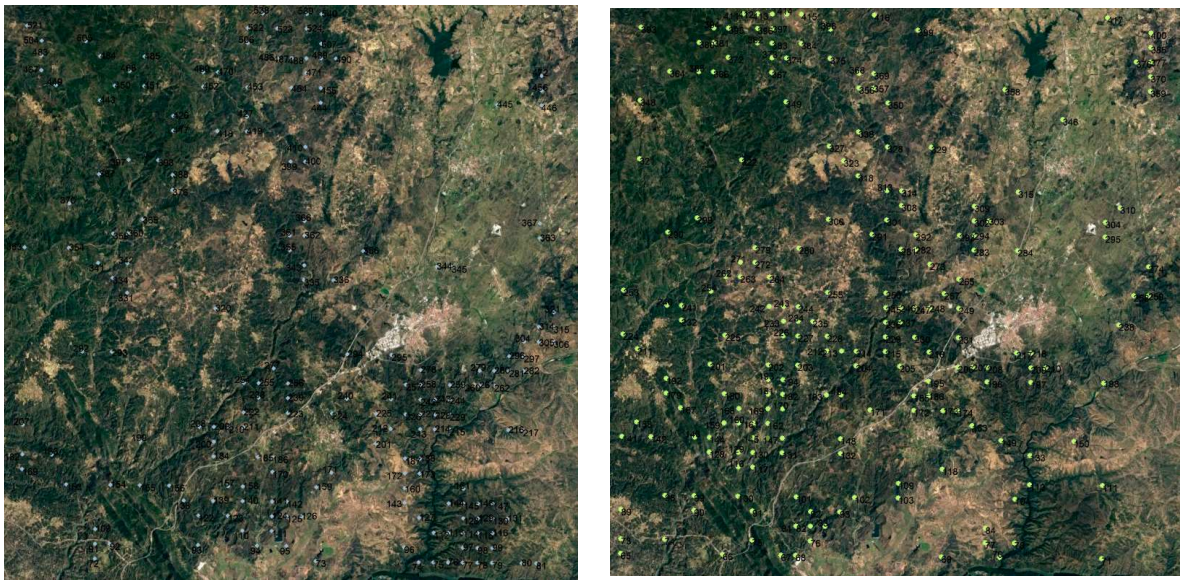

(**a**) (**b**)

Figure A2. Study area —Google Earth imagery (26 May 2023) with: (**a**) sample points in eucalypts areas (n = 197); and (**b**) shrubland areas (n = 227).

References

1. Avitabile, V.; Herold, M.; Henry, M.; Schmullius, C. Mapping biomass with remote sensing: A comparison of methods for the case study of Uganda. *Carbon Balance Manag.* **2011**, *6*, 7. [CrossRef] [PubMed]
2. Motlagh, M.G.; Kafaky, S.B.; Mataji, A.; Akhavan, R. Estimating and mapping forest biomass using regression models and Spot-6 images (case study: Hyrcanian forests of north of Iran). *Environ. Monit. Assess.* **2018**, *190*, 352. [CrossRef] [PubMed]
3. Thakur, T.K.; Swamy, S.L.; Bijalwan, A.; Dobriyal, M.J.R. Assessment of biomass and net primary productivity of a dry tropical forest using geospatial technology. *J. For. Res.* **2019**, *30*, 157–170. [CrossRef]
4. Massey, R.; Berner, L.T.; Foster, A.C.; Goetz, S.J.; Vepakomma, U. *Remote Sensing Tools for Monitoring Forests and Tracking Their Dynamics BT-Boreal Forests in the Face of Climate Change: Sustainable Management*; Girona, M.M., Morin, H., Gauthier, S., Bergeron, Y., Eds.; Springer International Publishing: Cham, Switzerland, 2023; pp. 637–655; ISBN 978-3-031-15988-6.
5. Thuy, H.L.T.; Tan, M.T.; Van, T.T.T.; Bien, L.B.; Ha, N.M.; Nhung, N.T. Using sentinel image data and plot survey for the assessment of biomass and carbon stock in coastal forests of Thai Binh Province, Vietnam. *Appl. Ecol. Environ. Res.* **2020**, *18*, 7499–7514. [CrossRef]
6. Araza, A.; Herold, M.; de Bruin, S.; Ciais, P.; Gibbs, D.A.; Harris, N.; Santoro, M.; Wigneron, J.P.; Yang, H.; Málaga, N.; et al. Past decade above-ground biomass change comparisons from four multi-temporal global maps. *Int. J. Appl. Earth Obs. Geoinf.* **2023**, *118*, 103274. [CrossRef]
7. Zhang, Y.; Liang, S.; Yang, L. A Review of Regional and Global Gridded Forest Biomass Datasets. *Remote Sens.* **2019**, *11*, 2744. [CrossRef]
8. Ferreira, S.; Monteiro, E.; Brito, P.; Vilarinho, C. Biomass resources in Portugal: Current status and prospects. *Renew. Sustain. Energy Rev.* **2017**, *78*, 1221–1235. [CrossRef]
9. Kumar, L.; Sinha, P.; Taylor, S.; Alqurashi, A.F. Review of the use of remote sensing for biomass estimation to support renewable energy generation. *J. Appl. Remote Sens.* **2015**, *9*, 097696. [CrossRef]
10. Ónodi, G.; Kertész, M.; Kovács-Láng, E.; Ódor, P.; Botta-Dukát, Z.; Lhotsky, B.; Barabás, S.; Mojzes, A.; Kröel-Dulay, G. Estimating aboveground herbaceous plant biomass via proxies: The confounding effects of sampling year and precipitation. *Ecol. Indic.* **2017**, *79*, 355–360. [CrossRef]
11. Forkel, M.; Carvalhais, N.; Verbesselt, J.; Mahecha, M.D.; Neigh, C.S.R.; Reichstein, M. Trend Change detection in NDVI time series: Effects of inter-annual variability and methodology. *Remote Sens.* **2013**, *5*, 2113–2144. [CrossRef]
12. Berra, E.F.; Fontana, D.C.; Kuplich, T.M. Tree Age As Adjustment Factor To Ndvi. *Rev. Árvore* **2017**, *41*, e410307. [CrossRef]
13. Gizachew, B.; Solberg, S.; Næsset, E.; Gobakken, T.; Bollandsås, O.M.; Breidenbach, J.; Zahabu, E.; Mauya, E.W. Mapping and estimating the total living biomass and carbon in low-biomass woodlands using Landsat 8 CDR data. *Carbon Balance Manag.* **2016**, *11*, 13. [CrossRef]
14. Santos, L.H.O.; Ramirez, G.M.; Roque, M.W.; de Lima Chaves, M.P.; Diaz, L.M.G.R.; Chaves, S.P. Correlação entre uniformidade e NDVI em povoamentos de Tectona grandis L. f. *BIOFIX Sci. J.* **2019**, *4*, 130. [CrossRef]
15. ICNF. *6° Inventário Florestal Nacional—IFN6. 2015. Relatório Final*; Instituto da Conservação da Natureza e das Florestas: Lisboa, Portugal, 2019. Available online: https://www.icnf.pt/api/file/doc/c8cc40b3b7ec8541 (accessed on 25 May 2023).

16. Águas, A.; Ferreira, A.; Maia, P.; Fernandes, P.M.; Roxo, L.; Keizer, J.; Silva, J.S.; Rego, F.C.; Moreira, F. Natural establishment of Eucalyptus globulus Labill. in burnt stands in Portugal. *For. Ecol. Manag.* **2014**, *323*, 47–56. [CrossRef]
17. Turnbull, J.W. Eucalypt plantations. *New For.* **1999**, *17*, 37–52. [CrossRef]
18. Alegria, C.; Pedro, N.; do Carmo Horta, M.; Roque, N.; Fernandez, P. Ecological envelope maps and stand production of eucalyptus plantations and naturally regenerated maritime pine stands in the central inland of Portugal. *For. Ecol. Manag.* **2019**, *432*, 327–344. [CrossRef]
19. FAO Group Reports. Group I: Bio-physical and environmental impacts of eucalyptus plantations. In Proceedings of the Regional Expert Consultation on Eucalyptus, Volume I, Bangkok, Thailand, 4–8 October 1993; White, K., Ball, J., Kashio, M., Eds.; FAO Regional Office for Asia and the Pacific: Bankok, Thailand, 1993.
20. Davidson, J. Ecological aspects of eucalyptus plantations. In Proceedings of the Regional Expert Consultation on Eucalyptus, Volume I, Bangkok, Thailand, 4–8 October 1993; White, K., Ball, J., Kashio, M., Eds.; FAO Regional Office for Asia and the Pacific: Bankok, Thailand, 1993; pp. 1–20. Available online: http://www.fao.org/3/a?ac777e/ac777e06.htm (accessed on 25 May 2023).
21. Fernandes, P.M. Combining forest structure data and fuel modelling to classify fire hazard in Portugal. *Ann. For. Sci.* **2009**, *66*, 415. [CrossRef]
22. Silva, J.; Moreira, F.; Vaz, P.; Catry, F.; Ferreira, P. Assessing the relative fire proneness of different forest types in Portugal. *Plant Biosyst.* **2009**, *143*, 597–608. [CrossRef]
23. Fernandes, P.M.; Luz, A.; Loureiro, C. Changes in wildfire severity from maritime pine woodland to contiguous forest types in the mountains of northwestern Portugal. *For. Ecol. Manag.* **2010**, *260*, 883–892. [CrossRef]
24. Gil, A.; Yu, Q.; Lobo, A.; Lourenço, P.; Silva, L.; Calado, H.; Jaume, T. Assessing the effectiveness of high resolution satellite imagery for vegetation mapping in small islands protected areas. *J. Coast. Res.* **2011**, *64*, 1663–1667, ISSN 0749-0208.
25. AFN. *Plano Municipal de Defesa da Floresta Contra Incêndios (PMDFCI)-Guia Técnico*; Autoridade Florestal Nacional: Lisboa, Portugal, 2012; Available online: https://www.icnf.pt/api/file/doc/034be5c061975659 (accessed on 23 June 2023).
26. Llorens, R.; Sobrino, J.A.; Fernández, C.; Fernández-Alonso, J.M.; Vega, J.A. A methodology to estimate forest fires burned areas and burn severity degrees using Sentinel-2 data. Application to the October 2017 fires in the Iberian Peninsula. *Int. J. Appl. Earth Obs. Geoinf.* **2021**, *95*, 102243. [CrossRef]
27. Fornacca, D.; Ren, G.; Xiao, W. Evaluating the best spectral indices for the detection of burn scars at several post-fire dates in a Mountainous Region of Northwest Yunnan, China. *Remote Sens.* **2018**, *10*, 1196. [CrossRef]
28. DGT Carta Administrativa Oficial de Portugal. Available online: https:/www.dgterritorio.gov.pt/search/dgt?keys=CAOP (accessed on 13 September 2022).
29. DGT. Carta de Uso e Ocupação do Solo. Registo Nacional de Dados Geográficos. SNIG. Direção-Geral do Território. Lisboa. Portugal. Available online: https://snig.dgterritorio.gov.pt/rndg/srv/por/catalog.search#/search?resultType=details&sortBy=referenceDateOrd&anysnig=COS&fast=index&from=1&to=20 (accessed on 13 September 2022).
30. DGT. *Especificações Técnicas da Carta de Uso e Ocupação do solo de Portugal Continental para 1995, 2007, 2010 e 2015. Relatório Técnico*; Direção-Geral do Território: Lisboa, Portugal. Available online: https://www.dgterritorio.gov.pt/sites/default/files/documentos-publicos/2019-12-26-11-47-32-0__ET-COS-2018_v1.pdf (accessed on 13 September 2022).
31. IPMA. Boletins Climatológicos de Portugal Continental. Instituto Português do Mar e da Atmosfera. Available online: https://www.ipma.pt/pt/publicacoes/boletins.jsp?cmbDep=cli&cmbTema=pcl&idDep=cli&idTema=pcl&curAno=-1 (accessed on 23 June 2023).
32. Navarro, G.; Caballero, I.; Silva, G.; Parra, P.-C.; Vázquez, Á.; Caldeira, R. Evaluation of forest fire on Madeira Island using Sentinel-2A MSI imagery. *Int. J. Appl. Earth Obs. Geoinf.* **2017**, *58*, 97–106. [CrossRef]
33. EOS NDVI FAQ: All You Need to Know about Index. Available online: https://eos.com/blog/ndvi-faq-all-you-need-to-know-about-ndvi/ (accessed on 13 September 2022).
34. Yang, Y.; Wu, T.; Wang, S.; Li, J.; Muhanmmad, F. The NDVI-CV Method for mapping evergreen trees in complex urban areas using reconstructed landsat 8 time-series data. *Forests* **2019**, *10*, 139. [CrossRef]
35. Vanclay, J.K. *Modelling Forest Growth and Yield. Applications to Mixed Tropical Forests*; CAB International: Wallingford, UK, 1994; 312p.
36. Tomé, M.; Barreiro, S.; Paulo, J.A.; Faias, S.P. Selecção de Equações para Estimação de Variáveis da Árvore em Inventários Florestais a Realizar em Portugal. Publicações FORCHANGE PT 9/2007. Lisboa, Portugal. 2007. Available online: https://www.isa.ulisboa.pt/cef/forchange/fctools/sites/default/files/pub/docs/equacoes-if_em_portugal.pdf (accessed on 23 May 2023).
37. Viana, H.; Aranha, J.; Lopes, D.; Cohen, W.B. Estimation of crown biomass of Pinus pinaster stands and shrubland above-ground biomass using forest inventory data, remotely sensed imagery and spatial prediction models. *Ecol. Modell.* **2012**, *226*, 22–35. [CrossRef]
38. Huang, S.; Yang, Y.; Wang, Y. A critical look at procedures for validating growth and yield models. In *Modelling Forest Systems*; Amaro, A., Reed, D., Soares, P., Eds.; CAB international: Wallingford, UK, 2003; pp. 271–293.
39. NASA JPL. NASA Shuttle Radar Topography Mission Global 1 Arc Second [Data Set]. Available online: http://doi.org/10.5067/MEaSUREs/SRTM/SRTMGL1.003 (accessed on 9 March 2018).
40. Lillesand, T.; Kiefer, R. *Remote Sensing and Image Interpretation*; John Wiley & Sons: Hoboken, NJ, USA, 1994; 376p.
41. Alegria, C. Vegetation Monitoring and Post-Fire Recovery: A Case Study in the Centre Inland of Portugal. *Sustainability* **2022**, *14*, 12698. [CrossRef]

42. Costa, R.; Fraga, H.; Fernandes, P.M.; Santos, J.A. Implications of future bioclimatic shifts on Portuguese forests. *Reg. Environ. Chang.* **2017**, *17*, 117–127. [CrossRef]
43. Chapungu, L.; Nhamo, L.; Gatti, R.C. Estimating biomass of savanna grasslands as a proxy of carbon stock using multispectral remote sensing. *Remote Sens. Appl. Soc. Environ.* **2020**, *17*, 100275. [CrossRef]
44. Filella, I.; Peñuelas, J.; Llorens, L.; Estiarte, M. Reflectance assessment of seasonal and annual changes in biomass and CO_2 uptake of a Mediterranean shrubland submitted to experimental warming and drought. *Remote Sens. Environ.* **2004**, *90*, 308–318. [CrossRef]
45. Castellnou, M.; Prat-Guitart, N.; Arilla, E.; Larrañaga, A.; Nebot, E.; Castellarnau, X.; Vendrell, J.; Pallàs, J.; Herrera, J.; Monturiol, M.; et al. Empowering strategic decision-making for wildfire management: Avoiding the fear trap and creating a resilient landscape. *Fire Ecol.* **2019**, *15*, 31. [CrossRef]